NASA Technical Memorandum 106851

IN-64

25P

Combining Comparison Functions and Finite Element Approximations in CFD

Kenneth J. Baumeister and Joseph F. Baumeister
Lewis Research Center
Cleveland, Ohio

March 1995

National Aeronautics and
Space Administration

N95-23614

Unclas

63/64 0044404

(NASA-TM-106851) COMBINING
COMPARISON FUNCTIONS AND FINITE
ELEMENT APPROXIMATIONS IN CFD
(NASA. Lewis Research Center) 25 p

COMBINING COMPARISON FUNCTIONS AND FINITE ELEMENT APPROXIMATIONS IN CFD

Kenneth J. Baumeister and Joseph F. Baumeister
National Aeronautics and Space Administration
Lewis Research Center
Cleveland, Ohio 44135

ABSTRACT

In a variety of potential flow applications, the modal element method has been shown to significantly reduce the numerical grid, employ a more precise grid termination boundary condition, and give theoretical insight to the flow physics. The method employs eigenfunctions to replace the numerical grid over significant portions of the flow field. Generally, a numerical grid is employed around obstacles with complex geometry while eigenfunctions are applied to regions to regions in the flow field where the boundary conditions can easily be satisfied. To handle a wider class of CFD problems, the present paper extends the modal element method to include comparison function approximations which do not satisfy the governing differential equation. To accomplish this task, a double modal series approximation and weighted residual constraints are developed to force the comparison functions to satisfy the governing differential equation and to interface properly with the finite element solution. As an example, the method is applied to the problem of potential flow in a channel with two-dimensional cylindrical like obstacles. The calculated flow fields are in excellent agreement with exact analytical solutions.

INTRODUCTION

Analytical-numerical approaches that help reduced computer storage requirement offer significant hardware and operational cost savings. The modal element method is one such analytical-numerical strategy to grid reduction. The method employs eigenfunctions to replace the numerical grid over significant portions of the flow field. Generally, a finite element grid is employed around obstacles with complex geometry while eigenfunctions are applied to regions where the boundary conditions can easily be satisfied. At the interface between the solution domains, continuity and gradient constraints couple the prescribed analytical and finite element solutions. In electromagnetics, acoustics and potential flow problems, the modal element method has been found to significantly reduce the numerical grid and provide a more precise grid termination boundary condition. More importantly, the method gives some theoretical insight to both the physical problem and the numerical analysis.

So far, the method has been restricted to linear problems where exact solutions (eigenfunctions) to the governing differential equation exist. In acoustics, Astley and Eversman (1981) and Baumeister and Kreider (1992) applied the modal element method to duct acoustic and scattering problems while Baumeister and Baumeister (1994) applied the method to potential flow over a cylinder. However, for more general CFD and acoustic problems, eigenfunction solutions do not exist. Therefore, the modal element method requires a wider class of approximate analytical functions to handle the more general cases.

The present paper extends the modal element method to include comparison function approximations (Meirovitch, 1967, pg. 140) that satisfy natural boundary conditions but do not satisfy the governing differential equation. To accomplish this task, a double modal series approximation is developed. Then, weighted residual constraints are developed to force this series to both satisfy the governing differential equation in the analytical domain and to interface properly with the finite element domain.

Emphasis in the paper is on the problem formulation although the analysis focuses on a specific geometry. As an example, the method is applied to potential flow in an infinitely long channel with two-dimensional cylindrical like obstacles. In the present paper, first the method of analysis and domain decomposition are discussed. The development of the analytical double series approximation for the potential immediately follows. Next, differential and subdomain interface constraints are developed. The finite element solution procedure and the flow geometry are then summarized. Finally, three example calculations are presented.

NOMENCLATURE

A	total dimensionless area of finite element domain
$A^{(e)}$	area of element e
A_m^-	eigenfunction modal amplitude, equation (32)
$A_{m,n}^-$	comparison function modal amplitude, equation (4)
$B_{m,n}^+$	comparison function modal amplitude, equation (12)
b	dipole strength, equation (30)
D	solution domain, equation (6)
$e(x,y)$	error, equation (5)
G	global matrix, equation (26)
h	dimensionless channel height, equation (2)
M	number of elements in finite element domain
M_c	number of transverse modes, equation (4)
M_{coef}	total number of modal coefficients used in comparison function, equation (23)
M_{pts}	number of grid points on interface S_a used in integration, equation (22)
m	mode number, equation (4)
m^*	weight mode number, equation (7)
N	number of nodes in finite element domain
N_c	number of exponential terms, equation (4)
$N^{(e)}$	local linear triangular interpolation function, $N^{(e)}(x,y)$, $[N_i^{(e)}(x_j,y_j) = \delta_{i,j}$ (i = 1,2,3; j = 1,2,3)]
n	exponential mode number, equation (4)

n^* exponential weight number, equation (7)

R   column vector, right hand side of global matrix equation, equation (26)

R_I global residual error at node I, equation (24)

S   line interface about finite element domain, see figure 3

S_a entrance plane, figure 3 and equation (24)

S_b exit plane, figure 3 and equation (24)

S^+ region exterior to S, equation (13)

S^- region interior to S, equation (13)

s   arc length parameter on S, equation (14)

U_∞^+ dimensionless free stream velocity, equation (2)

$U_\infty^{+\#}$ normalizing velocity, equation (2)

$W_I^{(e)}$ local weight function associated with node I, equation (24)

W_{m^*,n^*} global and interface weight function, equation (7)

x   dimensionless axial distance, equation (2)

x_{in} starting position of finite element grid, see figure 2

x_o axial intercept of obstacle, see figure 1

x_{out} ending position of finite element grid, see figure 2

y   dimensionless transverse distance, equation (2)

y_o height of obstacle, see figure 1

α axial decay constant, equation (4)

∇^2 Laplace operator

δ_{IJ} Kronecker delta ($\delta_{IJ} = 1$ for I = J; $\delta_{IJ} = 0$ for I $\neq$ J)

Φ column solution vector, equation (27)

ϕ dimensionless potential, equation (2)

Subscripts:

a   analytical solution entrance domain, see figure 3

b   analytical solution exit domain, see figure 3

I   global node index in finite element domain

I_s global node index for interface S, equation (17)

i   local element index, discussion of equation (25)

j   local element node index, equation (25)

Superscript:

~   approximate solution

dimensional quantity

$\overline{(\ )}$ average value

(e)   element value

METHOD OF ANALYSIS

The present study adapts modal element comparison functions to compute the potential flow field in a duct with two-dimensional cylindrical like obstacles, as shown in figure 1. The exact shape of the obstacle is defined by an infinite row of doublets transverse to a uniform flow (Kirchhoff, 1985). For obstacles less than half the height of the duct, its shape is nearly a circular cylinder. For this obstacle an exact solution for the flow field exists for validating the theoretical results. The detailed shape of the obstacle and the exact solution for the potential will be described later in this report.

For this configuration, a uniform velocity profile U_∞^+ is assumed to exist far upstream. For inviscid and irrotational two-dimensional flow, the dimensionless potential equation governs;

$$\nabla^2 \phi = 0 \tag{1}$$

where the following dimensionless variables are employed:

$$x = \frac{x^{\#}}{h^{\#}} \qquad y = \frac{y^{\#}}{h^{\#}}$$

$$h = \frac{h^{\#}}{h^{\#}} = 1 \qquad U_{\infty}^{+} = \frac{U_{\infty}^{+\#}}{U_{\infty}^{+\#}} = 1 \qquad\qquad (2)$$

$$\phi = \frac{\phi^{\#}}{U_{\infty}^{+\#} h^{\#}}$$

The superscript # indicates a dimensional variable. The channel height $h^{\#}$ is used as the characteristic dimension. The superscript + indicates the direction of the velocity in the + x direction. All symbols are defined in the nomenclature.

The common numerical approach to this problem (Chung, 1978 or Hilton and Owen, 1979) is to extend the grid far upstream and downstream of the obstacle, as shown in figure 2. Here, the assumption of uniform velocity at the grid termination is valid. Generally, a large entrance and exit grid region must be selected. The leading edge of the obstacle is defined by x_0 while the inlet and exit positions of the grid are defined by x_{in} and x_{out} respectively. Symmetry about the cylinder was not used allowing the computer program to handle a greater variety of problems.

In contrast to the conventional approach, figure 3 displays the modal element grid for this problem. The infinite spatial problem domain is divided into three subdomains, the bounded finite element domain, which is characterized by the cylindrical obstacle and the surrounding unbounded uniform channel entrance and exit domains. The velocity potential is represented approximately in the grid based domain by a finite element solution and will be represented analytically by a comparison trial function approximation in the uniform semi-infinite entrance and exit domains.

The finite element domain contains a nodal grid system that covers the region of complicated geometry. Linear triangular elements are used and the subdomain interface is approximated by piecewise linear segments. In the finite element domain, an approximate solution for the velocity potential is calculated by the Galerkin method. In the analytical domains, which extends to ± infinity, a double series expansion for the velocity potential is developed. The modal element method couples the analytical and numerical solutions by imposing continuity on the potential and velocity at the interface between the subdomains shown in figure 3. This coupling results in a single matrix equation. The series coefficients and the potential at the finite element nodes are calculated simultaneously, yielding a global representation of the potential field.

COMPARISON FUNCTION SOLUTION

Meirovitch (1967) suggest using comparison trial functions (satisfies geometric and natural boundary conditions) for approximate solutions to partial differential equations. In general, the trial function will depend on the geometry of the problem under consideration. Consider the entrance portion of the duct upstream to the duct obstruction as shown in figure 3 for $x < x_{in}$. For this flow field, the present solution will employ comparison trial functions which satisfy the natural boundary conditions along the upper wall and symmetry centerline for full cylinder in duct, namely that the transverse gradient of the velocity is zero:

$$v = \frac{\partial \phi}{\partial y} = 0 \quad \text{at} \quad y = 0 \ \& \ y = h = 1 \tag{3}$$

Therefore, in the entrance region a of figure 3, the comparison trial function will be assumed in the form

$$\tilde{\phi}_a = U_\infty^+ x + A_o^- + \sum_{m=1}^{M_c} \left(\sum_{n=1}^{N_c} A_{m,n}^- e^{n\alpha(x - x_{in})} \right) \cos(m\pi y) \tag{4}$$

The subscript a indicates that this function applies to spatial domain a of figure 3. The tilde above the function ϕ indicates that it is an approximate estimate of the solution. The first term represents the boundary condition on velocity at - infinity. The second A_o^- constant term is included since it is a solution of the governing equation (1). The terms represented by the double summation will blend the distorted potential around the obstacle into the uniform potential upstream. In the summation, the trigonometric terms cos (m π y) will be called a mode, similar to the terminology used in acoustics. The modal shapes represented by cos (m π y), as seen in figure 4, satisfies the natural boundary condition as given by equation (3).

For generality and ease in later integrations, the x dependance of each transverse mode cos(m Π y) is assumed exponential in form in equation (4) with the decay factor nα. Decay will occur since the value of $(x - x_{in})$ will always be a negative quantity in the exponential term of equation (4), since $(x - x_{in})$ has a negative value in the analytical entrance region shown in figures 1 and 3. For the problem under consideration, the transverse modes cos(m π y) will decay in a specific fashion which depends on the size of the cylindrical like obstacle shown in figure 1. The accuracy of equation (4) to predict this decay will depend on the total number of chosen exponential terms N_c and the chosen (known) value of α.

A total of N_c decay exponentials will be available to approximate the decay for each assumed transverse mode cos(m π y). In effect, a spectrum of decay factors, as shown in figure 5, is applied to each m th mode in equation (4). This spectrum is represented by the summation on n which is associated with the exponential terms in equation (4). For an acceptable numerical solution, the analysis must determine the proper value of the unknown modal coefficient $A_{m,n}$ for each assumed exponential decay factor n α shown in figure 5. The numerical constraints to be developed later will force the correct axial decay of each mode represented by cos(m π y).

The double series expansion given by equation (4) does not satisfy the governing differential equation (1). Substituting equation (4) into the governing equation (1) yields

$$\nabla^2 \tilde{\phi}_a = \sum_{m=1}^{M_c} \sum_{n=1}^{N_c} A_{m,n}^- \left[\left(n^2 \alpha^2 - m^2 \pi^2 \right) e^{n\ \alpha(x - x_{in})} \cos(m\pi y) \right] = e(x, y) \tag{5}$$

For the special case with $\alpha = \pi$ and $A_{m,n}^- = A_m^- \delta_{m,n}$ where $\delta_{m,n}$ is the Kronecker delta symbol, equation (4) reduces to the eigenfunction solution and the error e(x,y) is identical to zero. This case will be used later to validate the general theory. However, for a general assumed value of α, an error e(x,y) exists throughout region a. Consequently, the coefficients in equation (4) must be constrained so that the governing equation (1) is satisfied in some approximate manner and the error minimized over the domain. The method of weighted residuals is used to constrain the coefficients. The residual error associated with equation (4) over the analytical domain a is expressed as

6

$$R_{m^*,n^*}^{D_a} = \int\limits_{x=-\infty}^{x_{in}} \int\limits_{y=0}^{1} W_{m^*,n^*} \nabla^2 \tilde{\phi}_a \; dy \; dx$$

$$m^* = 1, 2, \ldots M_c \tag{6}$$

$$n^* = 1, 2, \ldots N_c$$

where the weight function is defined as

$$W_{m^*,n^*} = e^{n^*\alpha(x-x_{in})} \cos(m^* \pi y) \tag{7}$$

The superscript * designates the particular weight index to differentiate it from the summation indices m and n used in equation (4). In contrast to FE weighted residual theory using local weight functions, the weight function used here is global in nature acting over the whole x and y domain.

The residual defined by equation (6) can not be set to zero, because the coefficients in equation (4) must also be constrained to match the continuity of potential at the interface S_a between the finite element and analytical domains. A total residual constaint will be defined later. This total residual will be set to zero. In addition, the constant A_0^- need not be constrained since it already satisfies the governing differential equation. An interface constraint to be presented later will set the value of A_0^-.

Substituting equations (5) and (7) into equation (6) and rearranging yields the following expression for the residual

$$R_{m^*,n^*}^{D_a} = \sum_{n=1}^{N_c} \int\limits_{x=-\infty}^{x_{in}} e^{(n^*+n)\alpha(x-x_{in})} \sum_{m=1}^{M_c} A_{m,n}^- (n^2\alpha^2 - m^2\pi^2) \int\limits_{y=0}^{1} \cos(m^* \pi y)\cos(m \pi y)dy \; dx$$

$$m^* = 1, 2, \ldots M_c \tag{8}$$
$$n^* = 1, 2, \ldots N_c$$

Noting that

$$\int\limits_{y=0}^{1} \cos(m^* \pi y)\cos(m \pi y) \; dy = \frac{1}{2}(m^* = m)$$

$$= 0 \; (m^* \neq m) \tag{9}$$

Substituting equation (9) into equation (8) yields

7

$$R_{m^*,n^*}^{D_a} = \frac{1}{2} \sum_{n=1}^{N_c} A_{m^*,n}^- (n^2\alpha^2 - m^{*2}\pi^2) \int_{x=-\infty}^{x_{in}} e^{(n^*+n)\alpha(x-x_{in})} \, dx$$

$$m^* = 1,2,\ldots\ldots M_c$$

$$n^* = 1,2,\ldots\ldots N_c \tag{10}$$

The m summation in equation (8) has a value only when m equals the chosen weight value m^*. Consequently, the orthogonality of the cosine has lead to the elimination of the summation on the m modes. The final step is to integrate the simple exponential integral to obtain

$$R_{m^*,n^*}^{D_a} = \frac{1}{2} \sum_{n=1}^{N_c} A_{m^*,n}^- \frac{(n^2\alpha^2 - m^{*2}\pi^2)}{\alpha(n^*+n)}$$

$$m^* = 1,2,\ldots\ldots M_c$$

$$n^* = 1,2,\ldots\ldots N_c \tag{11}$$

Shortly, this equation will be combined with an interface equation to effectively constrain equation (4) to satisfy both the differential equation and join properly with the finite element solution.

For the exit duct where $x > x_{out}$, a similar analytical potential is developed in terms of constant $B_{m,n}^+$ as defined by

$$\tilde{\phi}_b = U_\infty^+ x + B_o^+ + \sum_{m=1}^{M_c} \sum_{n=1}^{N_c} B_{m,n}^+ e^{-n\alpha(x-x_{out})} \cos(m\pi y) \tag{12}$$

which gives a similar residual equation.

INTERFACE CONDITIONS

At the interface S between the finite element domain and the analytical domains, the local continuity of potential can be expressed as

$$\phi\big|_{s^+} - \phi\big|_{s^-} = 0 \tag{13}$$

A residual error is associated with matching the analytical potential in equation (4) to the value of the potential in the finite element domain along interface S_a in figure 3. This residual can be expressed numerically by an integral weighting procedure (Baumeister & Baumeister 1994) as follows:

$$R^{S_a}_{m*,n*} = \oint_{\substack{y=1 \\ y=0}} S_a W_{m*,n*}[\phi - \tilde{\phi}_a]\,ds$$

(14)

$$m* = 1,2,\dots,M_c$$

$$n* = 1,2,\dots,N_c$$

where the weight function is given by equation (7). Again, the superscript * designates the particular weight index to differentiate it from the trial function indices' m and n used in equation (4).

Substituting equation (4) and (7) into equation (14) and rearranging, yields

$$R^{S_a}_{m*,n*} = -[U^+_\infty x + A^-_o] \oint_{\substack{y=1 \\ y=0}} S_a \cos(m*\pi y)\,dy - \sum_{m=1}^{M_c}\left(\sum_{n=1}^{N_c} A^-_{m,n}\right) \oint_{\substack{y=1 \\ y=0}} S_a \cos(m*\pi y)\cos(m\pi y)\,dy$$

$$+ \oint_{\substack{y=1 \\ y=0}} S_a \cos(m*\pi y)\phi\,dy$$

(15)

$$m* = 1,2,\dots,M_c$$

$$n* = 1,2,\dots,N_c$$

The exponential terms have been evaluated at x_{in} so that the value of the exponential are identical to unity. Thus, the exponentials due not appear in equation (15). Because of the harmonic properties of the cosine, the first integral in equation (15) is zero. Again for the second integral, the orthogonal properties of the cosine, equation (9), yield nonzero integral values only when m is equal to the weight $m*$. Thus, the summation on m can be eliminated from the above equation to give

$$R^{S_a}_{m*,n*} = -\left(\sum_{n=1}^{N_c} 0.5 A^-_{m*,n}\right) + \oint_{\substack{y=1 \\ y=0}} S_a \cos(m*\pi y)\phi\,dy$$

(16)

$$m* = 1,2,\dots,M_c$$

$$n* = 1,2,\dots,N_c$$

In the integral in equation (16), ϕ is a function of y prescribed by the finite element nodal points on the interface surface S_a. It suffices to apply a simple quadrature to obtain acceptable results when evaluating equation (16). S_a is divided into subintervals centered at points (x_{Is}, y_{Is}), which correspond to finite element boundary nodes introduced later in the paper. The nodes are evenly spaced on the boundary with the index I_s. Once the number of modes M_c has been assumed (as defined in equation (4)) the number of nodes on S_a is set greater or equal to $6M_c$ to adequately resolve all the harmonic terms in equation (16).

9

Applying the midpoint rule to the chosen nodes gives

$$R^{S_a}_{m*,n*} = -\left(\sum_{n=1}^{N_c} 0.5 A^-_{m*,n}\right) + \sum_{I_s=1}^{M_{pts}} \cos\left(m * \pi\, y_{I_s}\right)\phi_{I_s}\, \Delta y_{I_s} \tag{17}$$

$$m* = 1, 2, \ldots, M_c$$

$$n* = 1, 2, \ldots, N_c$$

where Δy is the distance between nodes except at the two end points. At the ends, Δy is half the distance between nodes.

Equation (17) is the residual error if the analytical potential and the finite element potential do not match on the boundary. Shortly, this interface residual will be combined with the differential equation residual to get the final constraint equations for the trial function coefficients. But first, the residual error for the lowest plane mode will be determined.

The method of residuals for the lowest plane mode A^-_0 is written as

$$R^{S_a}_0 = \oint_{y=0}^{y=1} S_a [\phi - \tilde{\phi}_a]\, ds = 0 \tag{18}$$

The weight used here is unity. The residual error in this case is set to zero. Substituting in the value of $\tilde{\phi}$ from equation (4) into equation (18) and rearranging yields

$$R^{S_a}_0 = -[U^+_\infty x_{in} + A^-_0]\oint_{y=0}^{y=1} S_a\, ds - \sum_{n=1}^{N_c}\sum_{m=1}^{M_c} A^-_{m,n} \oint_{y=0}^{y=1} S_a\, \cos(m\,\pi\,y) + \oint_{y=0}^{y=1} S_a\, \phi\, ds = 0 \tag{19}$$

The first integral is identical to 1. Because of harmonic properties of the cosine, the second integral is identical to zero. The third integral is integrated numerically as before in equation (17). Thus, the interface constraint on the lowest order coefficient plane mode A^-_0 becomes

$$A^-_0 - \sum_{I_s=1}^{M_{pts}} \phi_{I_s} \Delta y_{I_s} = -U^+_\infty x_{in} \tag{20}$$

A similar set of equations can be written for the outlet b region coefficients.

TOTAL RESIDUAL CONSTRAINTS

The weight residual approach will be made to constrain the trial function constants in equation (4) so that they satisfy both the differential equation and the interface constraint simultaneously. The domain and line residuals are summed and set to zero as follows:

10

$$R^D_{m*,n*} + R^S_{m*,n*} = 0 \tag{21}$$

$$m* = 1, 2, \ldots, M_c$$
$$n* = 1, 2, \ldots, N_c$$

There must be one residual equation for every unknown constant $A_{m,n}$ following the summation signs in equation (4). Thus, $M_c \times N_c$ residual equations are required. These $M_c \times N_c$ equations, represented by equation (21), simultaneously satisfy both the differential equations and the interface condition for the higher order modes on the right hand side of the summation signs in equation (4). Substituting equations (11) and (17) into equation (21) and rearranging yields

$$\sum_{n=1}^{N_c} 0.5 \left(1 - \frac{\left(n^2 \alpha^2 - m^{*2} \pi^2\right)}{\alpha(n*+n)} \right) A^-_{m*,n} - \sum_{I_s=1}^{M_{pts}} \cos\left(m* \pi \, y_{I_s}\right) \phi_{I_s} \Delta y_{I_s} = 0$$

$$m* = 1, 2, \ldots, M_c \tag{22}$$

$$n* = 1, 2, \ldots, N_c$$

One additional equation, however, is needed for the unknown lowest order mode coefficient A^-_0. But, the differential equation residual associated with A^-_0 is identical to zero. Therefore, the total residual is simply equation (20). Thus, the total number of auxiliary residual equations is now defined as M_{coef} and is equal to

$$M_{coef} = 1 + M_c \times N_c \tag{23}$$

These equations represented by equations (20) and (22) are later combined with the finite element equations to form a matrix system that yields values of all the unknowns ϕ_I values at the FE nodes as well as the comparison function constants $A^-_{m,n}$. An additional set of residual equations similar to equation (22) is required to determine the $B^+_{m,n}$ unknowns as defined in equation (12). The $B^+_{m,n}$ coefficient determine the potential in the exit portion of the duct region shown in figure 3.

FINITE ELEMENT SOLUTION

The finite element domain, with total area A, is divided into M discrete triangular elements, $A^{(e)}$, $e = 1, 2, \ldots, M$, defined by N corner nodal points (x_I, y_I), $I = 1, 2, \ldots, N$. The corner nodes for element area $A^{(e)}$ are denoted $(x_1^{(e)}, y_1^{(e)})$, $(x_2^{(e)}, y_2^{(e)})$, and $(x_3^{(e)}, y_3^{(e)})$. The unknown potential ϕ_I is defined at node I. To determine the finite element difference equations for the potential at the nodes, application of the weak form of the weighted residuals to equation (1) yields

$$0 = R_I = \sum_{e=1}^{M} \left[\iint_{A^{(e)}} \left(\nabla W_I^{(e)} \cdot \nabla \tilde{\phi}^{(e)} \right) dA - \overline{\left(-\frac{\partial \phi_a}{\partial x} \right)}_{S^{(e)}} \int_{S^{(e)} \text{IS}_a} W_I^{(e)} ds - \overline{\left(\frac{\partial \phi_b}{\partial x} \right)}_{S^{(e)}} \int_{S^{(e)} \text{IS}_b} W_I^{(e)} ds \right]. \tag{24}$$

$$(I = 1, 2, 3, \ldots\ldots N)$$

Equation (24) is the standard weight residual representation of the nodal difference equations for the Laplace equation. A detailed derivation of equation (24) can be found in Baumeister and Baumeister (1994) or in standard text books (Chung, 1978 or Hinton and Owen 1979).

To evaluate the integrals in equation (24), it is necessary to represent $\phi(x,y)$ locally. Let $N_j^{(e)}$, $j = 1,2,3$, be the local linear shape functions for linear triangular elements associated with each corner node (defined in Hinton and Owen, 1979, pg. 180), so that

$$\tilde{\phi}^{(e)}(x,y) = \sum_{j=1}^{3} N_j^{(e)}(x,y)\phi_j^{(e)} = \left[N^{(e)}(x,y) \right]\left\{ \phi^{(e)} \right\}. \tag{25}$$

Also implement the Galerkin method—when the global index I equals the local node index i associated with node $(x_i^{(e)}, y_i^{(e)})$, let $W_I^{(e)}$ equal the local shape function $N_i^{(e)}$. The global shape function W_I is assumed to be identically zero for any element where node I does not appear (simple pyramid weight approximation); thus, the line integrals in equation (24) vanishes unless node I is on the boundary S_a or S_b.

The nodal difference equations represented by equation (24) are formed by performing the usual element by element summation as presented in introductory Finite Element texts. The natural boundary conditions are represented by the gradient of the analytical potential in equation (24). These gradient terms can be evaluated directly from equations (4) and (12) in terms of the unknown amplitude coefficients A^- and B^+. This insures continuity of the velocity at the interface between the analytical and finite element domains.

GLOBAL MATRIX EQUATION

The form of the global matrix equation is obtained by combining the finite element difference equations described by equation (24) along with the comparison function "difference" equations (20) and (22) and their exit equivalent in region b. The global matrix equation has the usual form.

$$[G]\{\Phi\} = \{R\} \tag{26}$$

where

$$\{\Phi\}^T = \{A_o^-, A_{1,1}^-, A_{1,2}^-, \ldots\ldots A_{1,N_c}^-, A_{2,1}^-, \ldots A_{2,N_c}^-,$$

$$\ldots\ldots\ldots\ldots\ldots A_{M_c,1}^-, A_{M_c,2}^-, \ldots A_{M_c,N_c}^-,$$

$$\phi_1, \phi_2, \phi_3, \phi_4, \phi_5, \phi_6, \ldots\ldots\ldots\ldots\ldots \phi_N, \tag{27}$$

$$B_o^+, B_{1,1}^+, B_{1,2}^+, \ldots\ldots B_{1,N_c}^+, B_{2,1}^+, \ldots B_{2,N_c}^+,$$

$$\ldots\ldots\ldots\ldots\ldots B_{M_c,1}^+, B_{M_c,2}^+, \ldots B_{M_c,N_c}^+ \}$$

12

The {R} column vector contains the free stream velocity terms present in equation (20) and the free stream velocity terms that enter equation (24) through the derivatives of ϕ_a and ϕ_b.

The matrix G has the following general form

$$
\begin{vmatrix}
A^{(11)} & \phi^{(12)} & 0 \\
A^{(21)} & \phi^{(22)} & B^{(23)} \\
0 & \phi^{(32)} & B^{(33)}
\end{vmatrix}
\begin{array}{l}
\text{equations (20) \& (22)} \\
\text{Finite Element Terms – equation (24)} \\
\text{exit equivalent of equations (20) \& (22)}
\end{array}
\qquad (28)
$$

The top and bottom rows in the matrix represent the contribution from the residuals which force the comparison function coefficients to satisfy the governing differential equation and interface matching condition, equations (20) and (22) and their exit equivalent. The middle row represents the finite element contribution from equation (24).

The submatrix $A^{(11)}$ is a full $M_{coef} \times M_{coef}$ matrix composed of the coefficients of the A_0^- and A_{mn}^- terms in eqs. (20) and (22). The submatrix $\phi^{(12)}$ is a sparse $M_{coef} \times N$ matrix composed of the coefficients of ϕ_I in equation (20) and (22). Only the nodes on the boundary line S_a have nonzero coefficients. The submatrices $\phi^{(32)}$ and $B^{(33)}$ are similar in form resulting from applying continuity at the exit interface.

The submatrix $A^{(21)}$ is an $N \times M_{coef}$ matrix composed of the coefficients of A_0^- and A_{mn}^- from the surface integral in equation (24). For each boundary node, there is a full row of terms in $A^{(21)}$. For interior nodes not on the boundary, the surface integral in equation (24) does not contribute to the difference equation. Consequently, there is a full row of zeros in $A^{(21)}$ at the interior nodes. A similar interpretation applies to $B^{(23)}$.

$\phi^{(22)}$ is a sparse, highly banded $N \times N$ matrix composed of the coefficients of ϕ_I resulting from the solution of equation (24). The global matrix equation, equation (26), is solved by a standard frontal solver program.

Finally, one additional constraint is required to keep the matrix equation (26) nonsingular. Up to this point, the difference equations are not completely independent, as discussed in Baumeister and Baumeister (1994). The potential must be given a value (grounded) at some nodal location in the finite element grid. For the purposes of this paper,

$$
\phi_I = 0.0 \quad \text{at} \quad x = 0.0 \quad y = 1.0 \qquad (29)
$$

GEOMETRICAL MODEL AND EXACT SOLUTIONS

The exact shape of the cylindrical like obstacle is defined by an infinite row of doublets transverse to a uniform flow (Kirchhoff 1985). Assuming an up stream value of $U_\infty^+ = 1$ and a channel of unit height, the height y as a function of x of the cylindrical like obstacle in figure 1 is given by

$$
0 = y - \frac{\pi b^2}{2} \frac{\sin(\pi y)}{\cosh(\pi x) - \cos(\pi y)} \qquad (30)
$$

Equation (30) is solved numerically by the bisection method for the height y of the obstacle as a function x and as a function of the assumed strength of the dipole parameter b. The following two values of b are used later in the examples:

b	x_0	y_0
0.5642	−0.5084	0.5000
1.9020	−1.1552	0.9000

Recall that the extremes of the obstacle x_0 and y_0 are defined in figure 1. The x_0 are negative quantities since the origin of the (x,y) coordinate system is directly under the center of the cylindrical like obstacle to the right of x_0. For dipole strength b equals 0.5642 the obstacle closely approximates a circular cylinder. In general, for obstacles less than half the height of the duct, the shape is nearly a circular cylinder.

The advantage of using this obstacle is that an exact solution exists for validating the theoretical results as given by (Baumeister and Baumeister, 1994)

$$\phi = x + \frac{\pi b^2}{2} \frac{\sinh(\pi x)}{\cosh(\pi x) - \cos(\pi y)} \tag{31}$$

Equation (31) will be compared graphically to the numerical examples presented later in the paper.

RESULTS AND COMPARISONS

To validate the method, three examples are presented for potential flow over a cylinder like obstacle described by equation (30). The first two example considers an obstacle that blocks 50 percent of the channel while the third example is concerned with an obstacle blocking 90 percent of the channel. For the examples to follow, recall that the channel has a dimensionless height of unity and the mean flow velocity is unity. The magnitude of the modal coefficients decrease rapidly for the higher order modes; thus, the summation parameters are chosen to be $M_c = 2$ and $N_c = 4$ for a comparison to the exact solution. Therefore, as defined in equation (23), $M_{coef} = 9$. Of course, for problems without an exact solution, the number of modes must be increased till the results converge.

Example 1.—Half Channel Obstruction - $\alpha = \pi$

Consider the potential flow over the cylinder with a b value of 0.5642, $x_0 = 0.5082$ and $y_0 = 0.5000$. In this example, the finite element region was placed directly over the obstacle as shown in figure 3 so that the start of the analytical domain x_{in} coincides with the beginning of the obstacle at x_0. As shown in figure 3, the finite element domain extends from -0.5082 to 0.5082. Thirteen nodes were used on the interface and eleven nodes along the surface of the obstacle for a total of 94 nodes and 142 elements, as shown in figure 6.

In figure 6, the velocity potential is plotted as a function of x along the upper wall, y = 1. The dashed line represents the potential on the duct wall without an obstacle. The modal element solutions (hollow boxes) are compared to the exact solution (solid line) given by equation (31). For −0.5082 < x < 0.5082, the values of potential at the finite element nodes are used to generate the solution. Also in figure 7, the numerical solution is generated from equations (4) and (12) using the numerically determined modal coefficients. Six separate values of the potential were calculated in each analytical region as shown in figure 7. Clearly, the modal element method gives good agreement with the exact results. Figure 8 shows the contour plot of the potential in both the analytical and finite element regions. The dash line in figure 8 shows the streamlines. Again, good agreement exists between the exact and the modal element results.

With $\alpha = \pi$ in this first example, the comparison function solution, equation (4), has imbedded the exact eigenfunction solution which has been shown to be (Baumeister and Baumeister, 1994):

$$\tilde{\phi}_a = U_\infty^+ x + A_o^- + \sum_{m=1}^{M_c} A_m^- e^{m\pi(x-x_{in})} \cos(m \pi y) \tag{32}$$

From equation (31) the exact values of the modal coefficients in equations (4) and (32) have been determined to have the following values:

$$A_o^- = -\frac{\pi b^2}{2} \tag{33}$$

$$A_{mn}^- = A_m^- \delta_{mn} \qquad \text{with} \qquad A_m^- \equiv -\pi b^2 e^{m\pi x_{in}} \tag{34}$$

For this symmetrical obstacle the B_m^+ modes are identical in magnitude to the A_m^- modes but of opposite sign. Because of the sharp decay predicted by equation (34), only the first two higher order modes need be calculated to obtain accurate results for the example problems considered.

To match the exact solution with $\alpha = \pi$ in this first example, the method of weighted residuals should set the coefficients to zero when $m \neq n$. This is indeed the case. The numerically calculated modal coefficients and the exact coefficients are:

Numerical Solution, equation (4)	Exact Solution, equations (33) & (34)
$A_0^- = -0.487$	$A_0^- = -0.50002$
$A_{1,1}^- = -0.196$	$A_{1,1}^- = -0.20247$
$A_{1,2}^- = +0.603 \times 10^{-4}$	$A_{1,2}^- = +0.0$
$A_{1,3}^- = -0.867 \times 10^{-4}$	$A_{1,3}^- = +0.0$
$A_{1,4}^- = +0.394 \times 10^{-4}$	$A_{1,4}^- = +0.0$
$A_{2,1}^- = +0.246 \times 10^{-5}$	$A_{2,1}^- = +0.0$
$A_{2,2}^- = -0.402 \times 10^{-1}$	$A_{2,2}^- = -0.40994 \times 10^{-1}$
$A_{2,3}^- = -0.186 \times 10^{-4}$	$A_{2,3}^- = +0.0$
$A_{2,4}^- = -0.858 \times 10^{-5}$	$A_{2,4}^- = +0.0$

As seen above, the numerically calculated and exact modal coefficients are in good agreement. This agreement accounts for the excellent match between exact theory (solid line) and the numerical results (square symbols) in the analytical regions shown in figures 7 and 8. The agreement occurs in both the analytical entrance and exit regions as well as in the finite element region direct on top of the obstacle.

Example 2.—Half Channel Obstruction - $\alpha = 2.5$

Example 2 has the same geometry and parameters as example 1 except $\alpha = 2.5$. In contrast to example 1, for $\alpha = 2.5$ the exact eigenvalue solution is not imbedded in the comparison function solution. In this case, only an approximate solution is possible. However, the numerical results are still in very good agreement with the exact results. To the eye, plots of the numerical results appear exactly as shown in figure 7 for the potential along the upper wall and in figure 8 for the contours of the potential. Thus, these numerical results are not presented in figure form. An explanation for this excellent agreement can be found by examining the coefficients of the comparison function expansion, equation (4).

The numerically calculated modal coefficients and the exact coefficient are:

Numerical Solution, equation (4)   Exact Solution, equations (33)

$A_0^- = -0.484$ $A_0^- = -0.50002 \times 10$

$A_{1,1}^- = -0.9489 \times 10^{-1}$

$A_{1,2}^- = -0.2041$

$A_{1,3}^- = +0.1553$

$A_{1,4}^- = -0.5326 \times 10^{-1}$

$A_{2,1}^- = +0.7332 \times 10^{-3}$

$A_{2,2}^- = -0.1516 \times 10^{-1}$

$A_{2,3}^- = -0.3056 \times 10^{-1}$

$A_{2,4}^- = +0.5649 \times 10^{-2}$

The numerical value of lowest order mode A_0^- is good agreement with the theoretical value. For the first transverse mode ($m = 1$), the product of the modal coefficient and its exponential damping factor are plotted in figure 9 for various axial mode numbers n. The abscissa is the distance from the interface between the finite element region and the analytical inlet region a. In addition, the solid line without symbols is a plot of the value of the axial component of the exact eigenfunction given in equation (32). An inspection of figure 9 reveals that the sum of the n axial components approximates the value of the axial component of the eigenfunction. This is shown explicitly in figure 10. The solid numerical points represent the sum of the curves shown in figure 9. Thus, even with a very coarse series approximation, the weighted residual approach adjusts the coefficients of the comparison function to match the exact eigenfunction.

Example 3.—Large Channel Obstruction - $\alpha = 2.5$

Consider the potential flow over the cylinder with a b value of 1.9020, $x_0 = -1.1552$ and $y_0 = 0.9000$. In this case, 90 percent of the channel has an obstruction as illustrated in figure 11. The grid was extended slightly in front of the obstacle to better resolve the steep slope of the obstacle near x_0. In this case, $x_{in} = -1.3984$ and $x_{out} = 1.3984$. Twenty one nodes were used on the interface and 132 nodes along the upper channel wall for a total of 1272 nodes and 2212 elements, as shown in figure 11.

In figure 12, the velocity potential is again plotted as a function of x along the upper wall, $y = 1$. The dashed line again represents the potential on the duct wall without an obstacle. The modal element solutions (hollow boxes) are compared to the exact solution (solid line) given by equation (31). In figure 12, for $-1.3984 < x < 1.3984$, the values of potential at the finite element nodes are used to generate the solution. Also in figure 12, the numerical solution is generated from equation (4) using the numerically determined modal coefficients. Similar to figure 8, the contour plots of the numerical potentials were in very good agreement with the theoretical values.

The numerically calculated modal coefficients and the exact coefficients are as follows:

Numerical Solution, equation (4)   Exact Solution, equation (33)

$A_0^- = -0.5671 \times 10^1$ $A_0^- = -0.5683 \times 10^1$

$A_{1,1}^- = -0.6801 \times 10^{-1}$

$A_{1,2}^- = -0.1465$

$A_{1,3}^- = +0.1115$

$A_{1,4}^- = -0.3828 \times 10^{-1}$

$A_{2,1}^- = +0.3633 \times 10^{-4}$

$A_{2,2}^- = -0.6749 \times 10^{-3}$

$A_{2,3}^- = -0.1250 \times 10^{-2}$

$A_{2,4}^- = +0.2165 \times 10^{-3}$

16

CONCLUDING REMARKS

The modal element method using comparison functions has been presented. The method has been applied to potential flow over a two-dimensional cylindrical like obstacle. In the example problems, the total flow domain is broken into three subdomains that are patched together. The potential field is represented by a finite element solution in the irregular subdomain next to the obstacle and by a comparison function expansion in the unbounded entrance and exit ducts. By the method of weighted residuals, the comparison function is simultaneously constrained to satisfy both the governing Laplace equation and the continuity of potential and velocity across the interface between the subdomains. The combined numerical and analytical results show excellent agreement with the corresponding exact solutions. The method is robust in that relatively coarse series approximations have developed very accurate results.

REFERENCES

Astley, R. J. , and Eversman, W., 1981, "Acoustic Transmission in Non-Uniform Ducts with Mean Flow, Part II: The Finite Element Method," Journal of Sound and Vibration, Vol. 74, pp. 103–121.

Baumeister, K. J. and Baumeister, J. F., 1994, "Modal Element Method for Potential Flow in Non-Uniform Ducts: Combining Closed Form Analysis With CFD," AIAA Paper 94–0813.

Baumeister, K. J. and Kreider, K. L., 1993, "Modal Element Method for Scattering of Sound by Absorbing Bodies," Transactions of the ASME, Jour. Vibrations and Acoustics, Vol. 115, pp. 314–323.

Chung, T.J., 1978, "Finite Element Analysis in Fluid Mechanics," McGraw-Hill, New York.

Hinton, E. and Owen, D. R. J., 1979, "An Introduction to Finite Element Computations" Pineridge Press, Swansea, U.K.

Kirchhoff, R. H., 1985, "Potential Flows- Computer Graphic Solutions," Marcel Dekker, Inc, New York.

Meirovitch, L., 1967, "Analytical Methods in Vibrations," Macmillan Company, London.
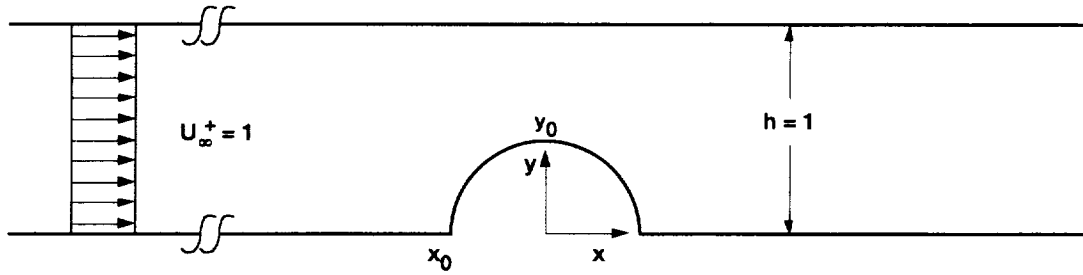
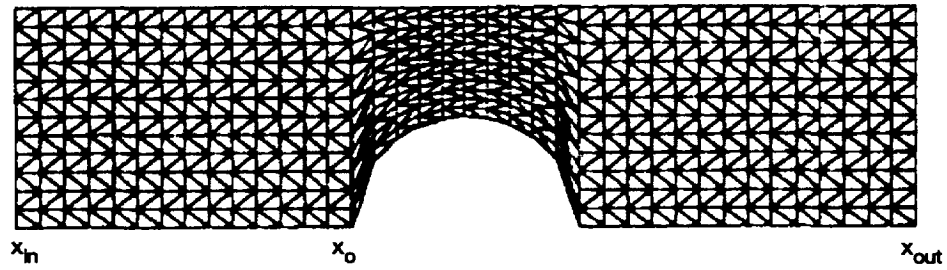Figure 1.—Flow field geometry.

Figure 2.— Conventional finite element discretization for flow around cylindrical object in channel.
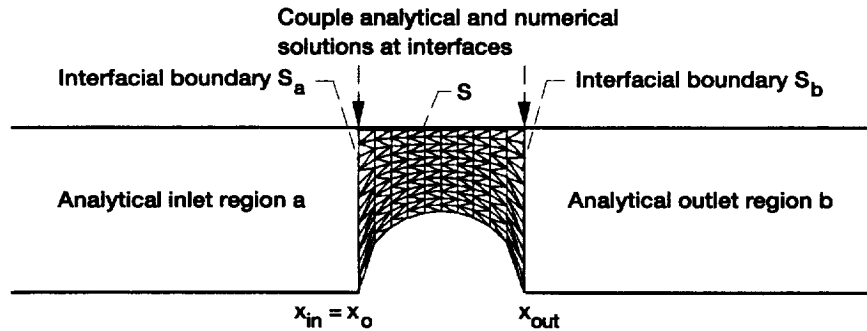

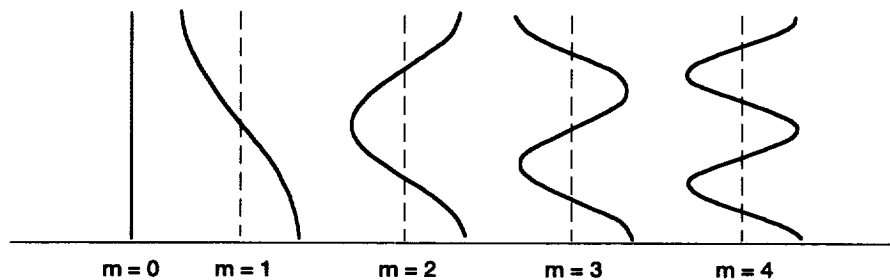Figure 3.—Modal element finite element discretization for flow around cylindrical object in channel.

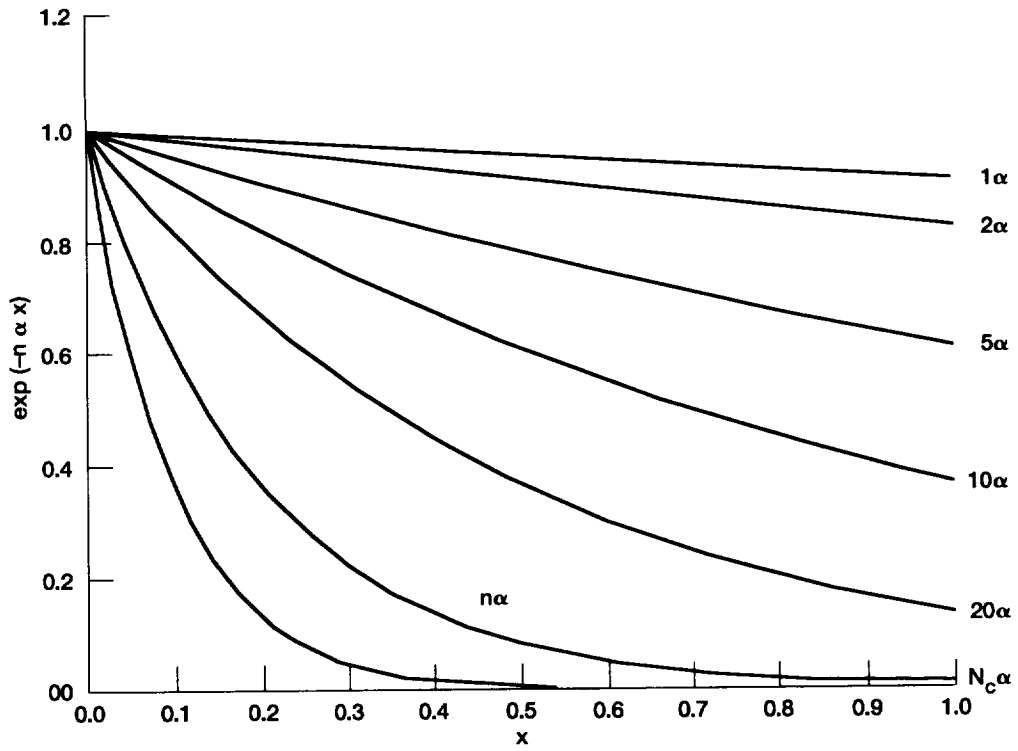Figure 4.—Transverse modal content in duct.

18

Figure 5.—Spectrum of exponential decay curves (α = 0.1 in illustration).
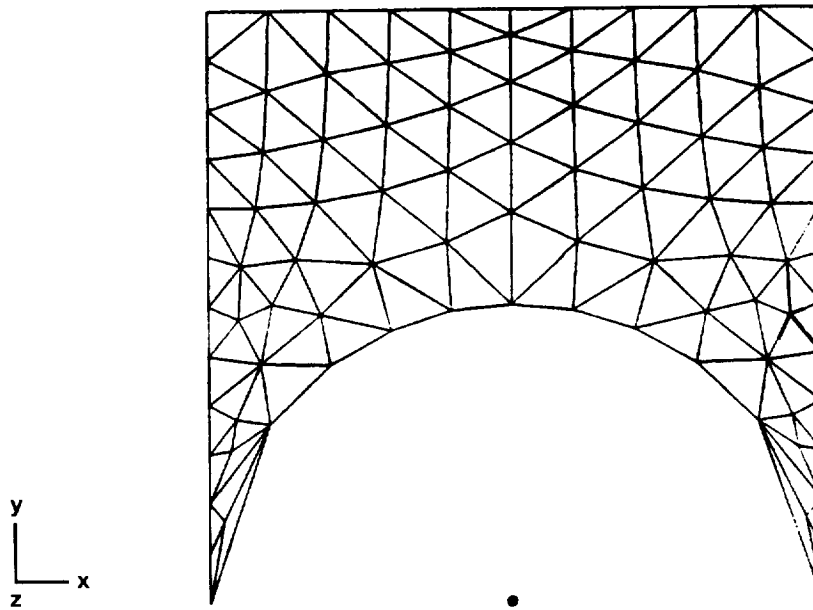

Figure 6.—Modal element finite element discretization for flow around cylindrical object in channel with $y_0 = 0.5$.
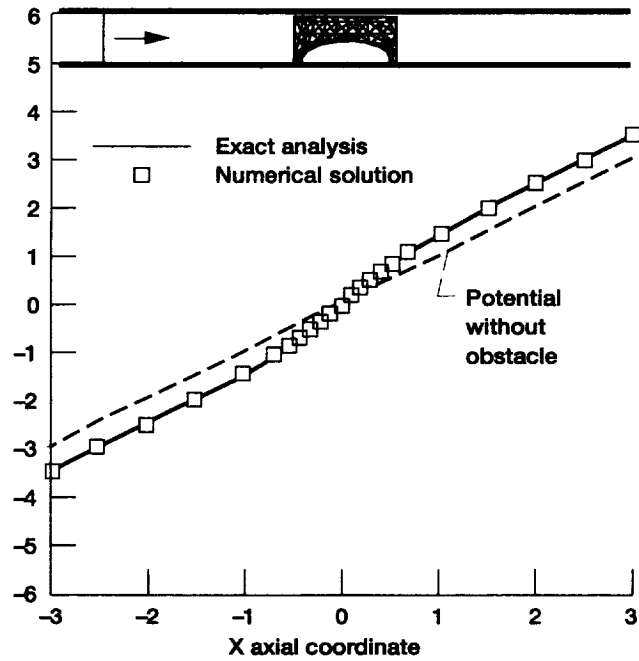
Figure 7.—Effect of a half channel obstruction on the potential along the upper wall ($\alpha = \pi$, $M_c = 2$, $N_c = 4$ with 94 nodes and 142 elements).
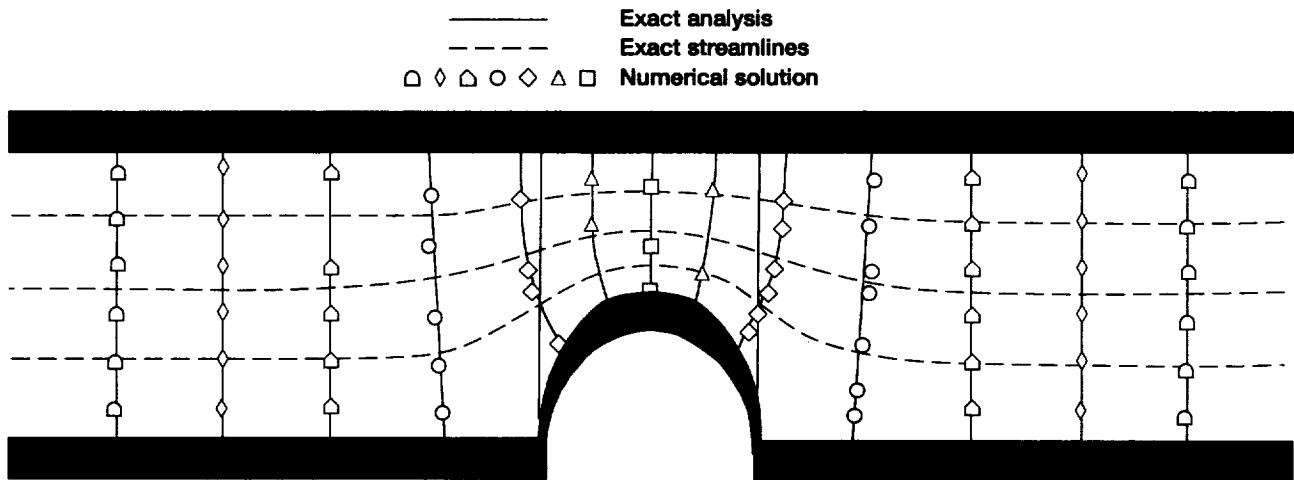
Figure 8.—Contour plots of the potential in both the finite element and the analytical regions for half the channel obstruction ($\alpha = \pi$, $M_c = 2$, $N_c = 4$ with 94 nodes and 142 elements).
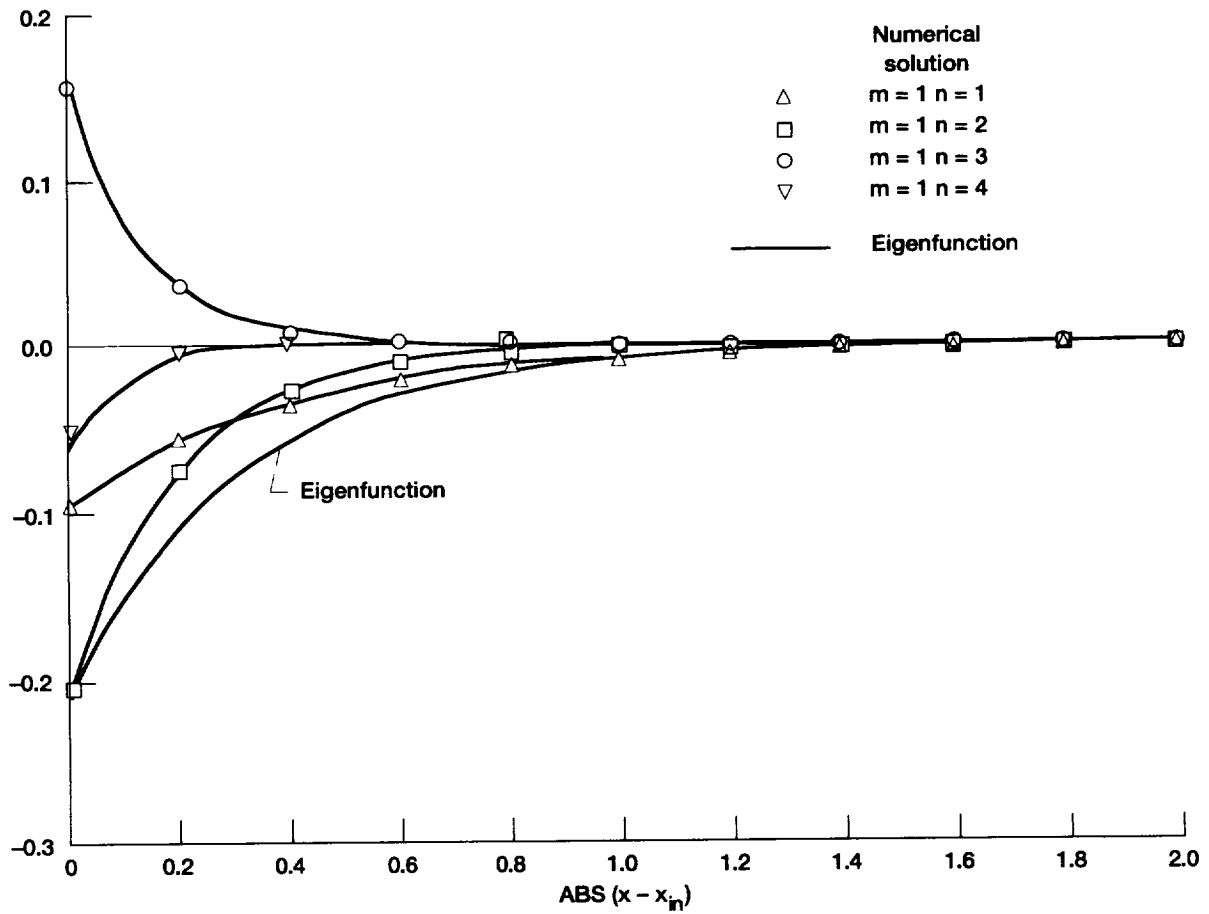
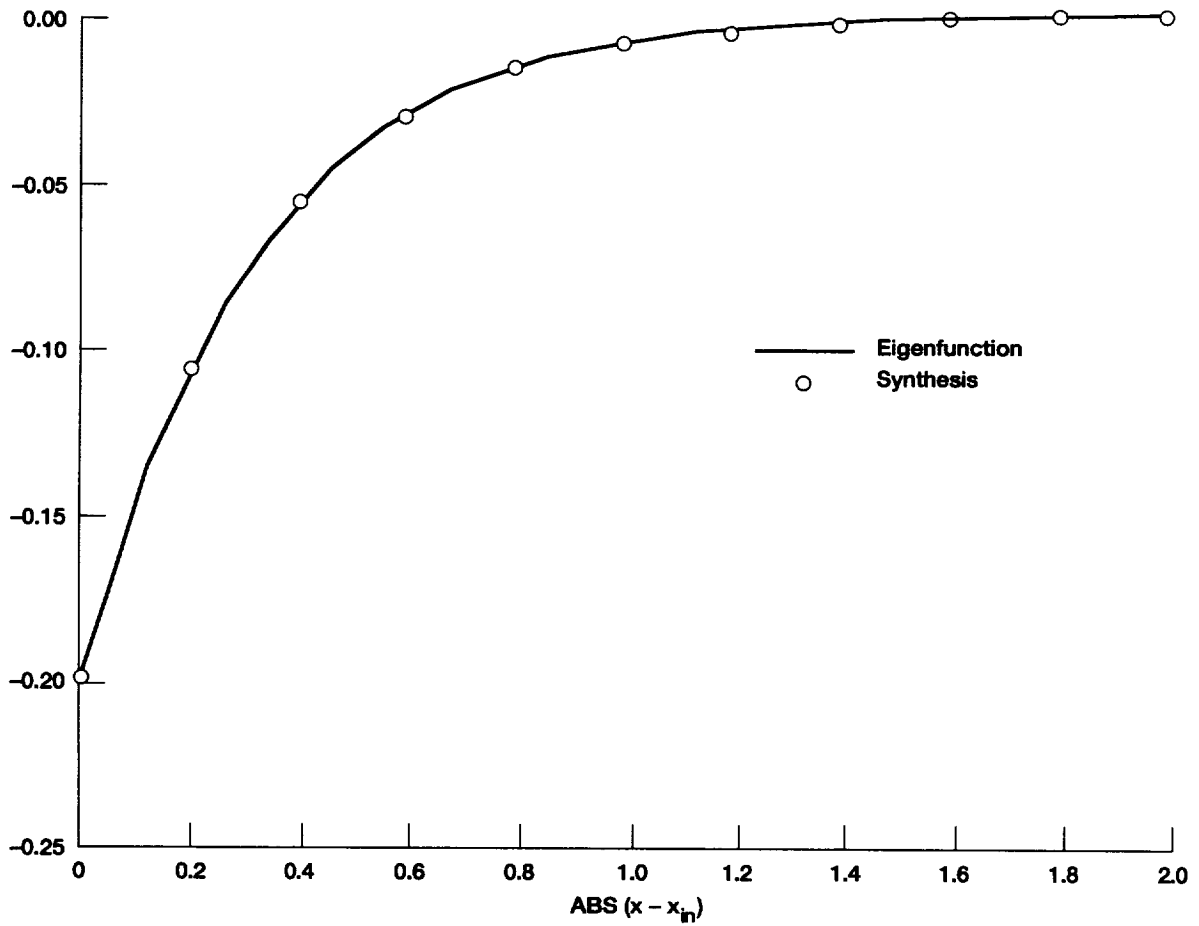Figure 9.—Axial components of transverse mode m = 1 for 50 percent channel blockage, alpha = 2.5.

Figure 10.—Axial mode synthesis for transverse mode m = 1 (50 percent channel blockage, alpha = 2.5).
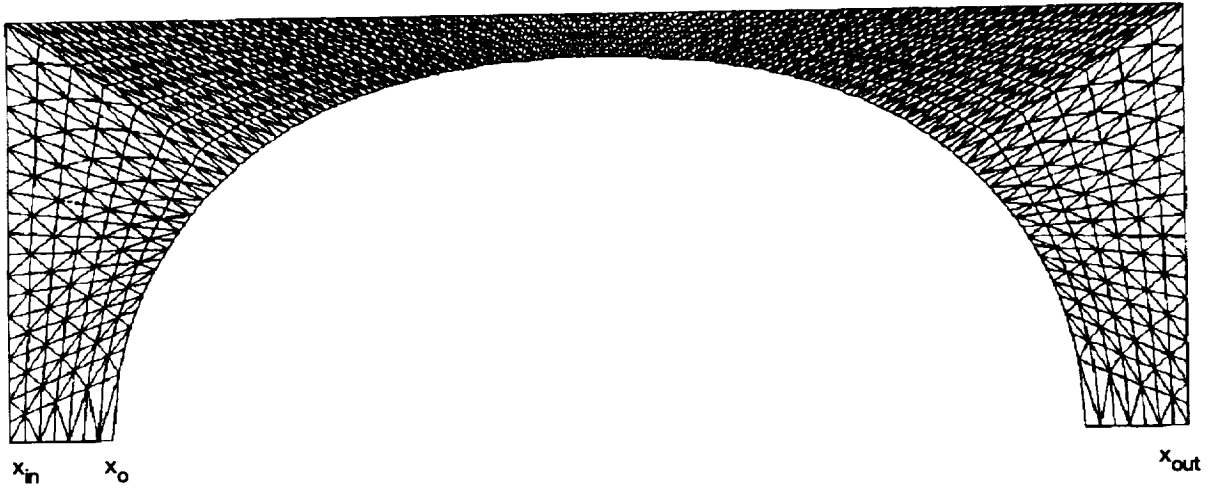
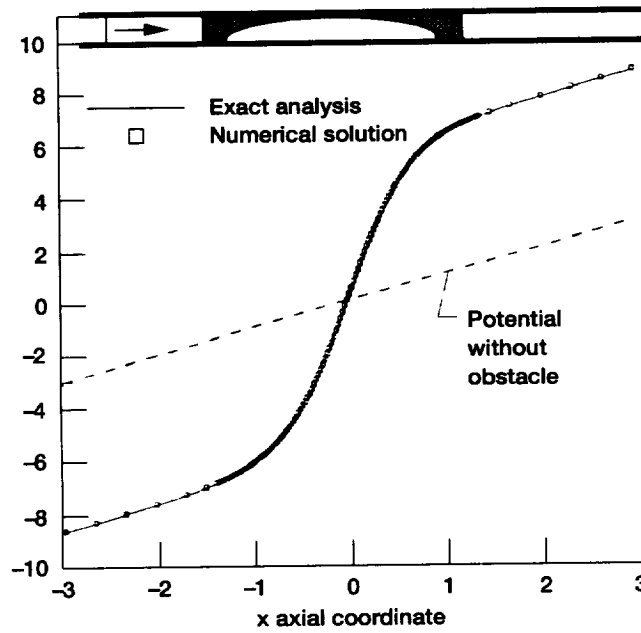Figure 11.—Modal element finite element discretization for flow around large cylindrical object in channel.

Figure 12.—Effect of a large channel obstruction on the potential along the upper wall (1272 nodes and 2212 elements).

23

REPORT DOCUMENTATION PAGE

Public reporting burden for this collection of information is estimated to average 1 hour per response, including the time for reviewing instructions, searching existing data sources, gathering and maintaining the data needed, and completing and reviewing the collection of information. Send comments regarding this burden estimate or any other aspect of this collection of information, including suggestions for reducing this burden, to Washington Headquarters Services, Directorate for Information Operations and Reports, 1215 Jefferson Davis Highway, Suite 1204, Arlington, VA 22202-4302, and to the Office of Management and Budget, Paperwork Reduction Project (0704-0188), Washington, DC 20503.

1. AGENCY USE ONLY (Leave blank)	2. REPORT DATE	3. REPORT TYPE AND DATES COVERED
	March 1995	Technical Memorandum

4. TITLE AND SUBTITLE

Combining Comparison Functions and Finite Element Approximations in CFD

5. FUNDING NUMBERS

WU–505–62–52

6. AUTHOR(S)

Kenneth J. Baumeister and Joseph F. Baumeister

7. PERFORMING ORGANIZATION NAME(S) AND ADDRESS(ES)

National Aeronautics and Space Administration
Lewis Research Center
Cleveland, Ohio 44135–3191

8. PERFORMING ORGANIZATION REPORT NUMBER

E–9440

9. SPONSORING/MONITORING AGENCY NAME(S) AND ADDRESS(ES)

National Aeronautics and Space Administration
Washington, D.C. 20546–0001

10. SPONSORING/MONITORING AGENCY REPORT NUMBER

NASA TM–106851

11. SUPPLEMENTARY NOTES

Responsible person, Kenneth J. Baumeister, organization code 2660, (216) 433–5886.

12a. DISTRIBUTION/AVAILABILITY STATEMENT

Unclassified - Unlimited
Subject Category 64

This publication is available from the NASA Center for Aerospace Information, (301) 621–0390.

12b. DISTRIBUTION CODE

13. ABSTRACT (Maximum 200 words)

In a variety of potential flow applications, the modal element method has been shown to significantly reduce the numerical grid, employ a more precise grid termination boundary condition, and give theoretical insight to the flow physics. The method employs eigenfunctions to replace the numerical grid over significant portions of the flow field. Generally, a numerical grid is employed around obstacles with complex geometry while eigenfunctions are applied to regions to regions in the flow field where the boundary conditions can easily be satisfied. To handle a wider class of CFD problems, the present paper extends the modal element method to include comparison function approximations which do not satisfy the governing differential equation. To accomplish this task, a double modal series approximation and weighted residual constraints are developed to force the comparison functions to satisfy the governing differential equation and to interface properly with the finite element solution. As an example, the method is applied to the problem of potential flow in a channel with two-dimensional cylindrical like obstacles. The calculated flow fields are in excellent agreement with exact analytical solutions.

14. SUBJECT TERMS

Finite element; Potential flow; Modes

15. NUMBER OF PAGES

25

16. PRICE CODE

A03

17. SECURITY CLASSIFICATION OF REPORT	18. SECURITY CLASSIFICATION OF THIS PAGE	19. SECURITY CLASSIFICATION OF ABSTRACT	20. LIMITATION OF ABSTRACT
Unclassified	Unclassified	Unclassified	

NSN 7540-01-280-5500